An Ultrahigh Pore Volume Drives Up the Amine Stability and Cyclic CO_2 Capacity of a Solid-Amine@Carbon Sorbent

Srinivas Gadipelli, Hasmukh A. Patel, and Zhengxiao Guo**

Energy-related burning of fossil fuels is responsible for two-thirds of the anthropological CO_2 emission that causes climate change.[1,2] As a result, there is heightened public pressure for divestment in fossil fuels, unless effective carbon capture and sequestration (CCS) technology is implemented as a short/medium-term solution.[3] Current CCS for postcombustion flue gas stream is based on liquid amine scrubbing, where the flue gas is passed through an aqueous amine solution.[3–5] However, the system suffers from a relatively high energy penalty due to limited surface utilization, easy degradation to harmful species, and high-temperature regeneration. In this regard, solid adsorbents with high accessible surface area, stability, and appropriate molecular binding energies are attractive to enhance the sorbent performance.[3–7] In particular, common porous physical adsorbents, such as zeolites, carbons, and metal–organic frameworks (MOFs), show great promise, especially for dry CO_2 adsorption.[7–9] Further chemical functionalization, e.g., attaching alkyl–amine groups on pore surfaces have been adopted to enhance the selective sorption of CO_2 and tolerance against humidity and other acidic gases in the effluent stream.[10–12]

Recently, physical immobilization of amines on a porous support via wet impregnation has been demonstrated as a simple route of achieving an effective CO_2 sorbent for flue-gas conditions.[13–15] A notable example is the amine@mesoporous silica system, where the achievable CO_2 capacities are directly related to the level of amine loading.[16–18] However, the amine loading is limited in such silica supports, due to its relatively low pore surface area, low pore volume, and the mainly 1D pore geometry. Attempt to increase the amine loading usually comes at the expense of amine efficiency due to excessive coating of multiple amine layers on particulate external surfaces. This ultimately compromises the sorbent performance, i.e., stability and lifetime, as desorption cycling leads to considerable amine leaching.[17–20] In addition, the size of the porous silica particles is mostly limited to the nano-/micrometer levels, which can easily plug/entrain the filters in fluidized beds.[21]

Dr. S. Gadipelli, Dr. H. A. Patel, Prof. Z. Guo
Department of Chemistry
University College London
London WC1H 0AJ, UK
E-mail: gsrinivasphys@gmail.com; z.x.guo@ucl.ac.uk

DOI: 10.1002/adma.201502047

Therefore, for practical implementation of solid-amine sorbents, it is critical to enhance sorption working capacity, amine stability over multiple regeneration cycles, and particle size of the porous support. In principle, these issues can be resolved if a suitable support monolith can be developed, which show both high surface area and high pore volume, to offer high amine loading and binding within the 3D interconnected network pores.[16,22–24] Though tetraethylenepentamine (TEPA) is preferred over polyethyleneimine (PEI) due to its favorable CO_2 uptake with a high amine concentration, the volatilization of TEPA is a serious issue compared with PEI.[11,18–20] Also if found suitable, a low-cost support is preferred. Here, we show a highly efficient CO_2 scrubber with TEPA impregnated in an MOF-derived carbon monolith (MDCM) that exhibits simultaneously high specific surface area (SSA $\approx$ 2700 m^2 g^{-1}) and ultrahigh hierarchical pore volume ($V_p \approx 5.35$ cm^3 g^{-1}). This is the first demonstration of such kind of porous supports that is capable of accommodating a record level of amine and maintaining the amine stability within the pores over several cycles. The system constantly shows over 200 mg g^{-1} of CO_2 adsorption capacity at simulated flue gas and practical conditions (humidified, 15% CO_2 balanced with N_2, uptake at 75 °C and desorption at 100 °C) over several repeated cycles, outperforming any known sorbents reported to date. It can be regarded as a new generation of CO_2 super scrubber. To strengthen our findings the results are comparatively discussed with amine@activated graphene oxide (ActGO) ($V_p \approx 1.9$ cm^3 g^{-1}) with small pore size distribution (PSD) of hierarchical pores and other literature on amine@silica with well-defined uniform pores.

Figure 1 shows the synthesis approaches and the porous structural characteristics of amine-loaded porous supports. Extraordinary advantage of the ultrahigh pore volume MDCM over other traditional MOF/activated carbon can be seen. Details of the synthesis of MOF-5 crystals, derived carbon monoliths, and ActGO are given in the Supporting Information (see the Experimental Section, Figure S1–S3, Supporting Information). MOF-5 (Zn_4O[benzene dicarboxylate]$_3$) shows a relatively high porosity ($V_p \approx 1.2$ cm^3 g^{-1} and SSA $\geq$ 3000 m^2 g^{-1}) with cubic framework nanopore cages around 1.2 nm. On a practical level, it is inexpensive and relatively easy to synthesize in large quantities, e.g., at room temperature by stirring or a solvothermal method with the precursors (Zn nitrate salt and benzenedicarboxylic acid) solvent (*N,N′*-diethylformamide) in a tightly capped vial at 100 °C for a day. A rapid microwave or sonochemical synthesis has also been applied. However, MOF-5 is not well received for the gas storage specifically due to its low molecular binding energy and uptake capacity.[7a] Importantly, it is highly sensitive to moisture and other flue gas containing acidic gases, which lead to degradation and complete collapse

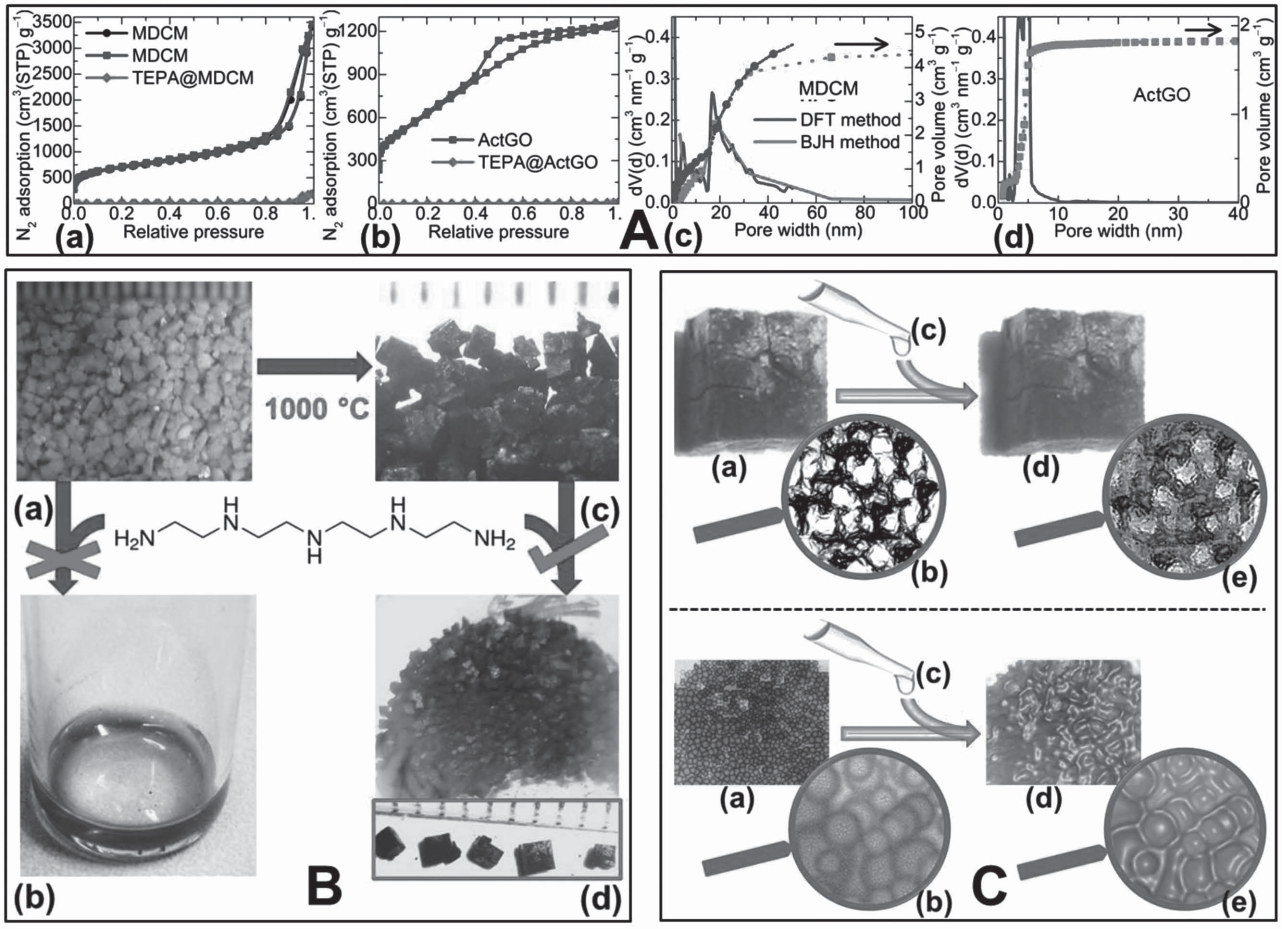

Figure 1. Synthesis and porosity characteristics of MDCM and ActGO before and after TEPA loading. A) (a, b) Nitrogen adsorption–desorption isotherms at 77 K and (c, d) derived PSD-V_p plots for (a, c) MDCM and (b, d) ActGO, pore-filling can be seen after TEPA impregnation. B) Digital photographs with millimeter scale bar for (a, b) MOF-5 and (c, d) MDCM before and after TEPA loading. C) Schematic illustrations of surface and pore textures of a single MDCM (above, a magnified photograph of (B)) and powdered ActGO (below) (a, b) before and (d, e) after (c) TEPA impregnation. In both cases, (b) and (e) are magnified versions of pore/surface textures. A pore-only confined and excess surface coated TEPA is seen in MDCM and ActGO, respectively, for a given 5 g $g^{-1}$of TEPA loading.

of the porosity.[8] As shown in Figure 1B the MOF-5 decomposes with amine impregnation.

Here, the readily synthesized MOF-5 structure is further exploited to obtain a much more stable and highly robust porous carbon (Figures S2–S5, Supporting Information). The MDCM is obtained by direct carbonization of MOF-5 at 1000 °C. As shown in Figure 1A the carbonization leads to a new generation of hierarchical micro- and mesopores with simultaneously high SSA of ≈2700 m^2 g^{-1} and ultrahigh V_p of 5.35 cm^3 g^{-1}; the latter is over four times greater than the V_p of MOF-5 and most of the commercial mesoporous silica, MCM-41 and SBA-15 (Table S1 and Figure S1, Supporting Information). Some fundamental insights into this structural transformation during carbonization of MOF and subsequent pore generation can be found in the literature.[23,25,26] The PSD shows predominantly hierarchical mesoscale porosities between 3 and 50 nm. The mesopores between 3 and 200 nm derived from the BJH method accounts over 4.65 cm^3 g^{-1}. The micropores (up to 3 nm by means of the DFT method) account for 0.6 cm^3 g^{-1} (Figure S4, Supporting Information). In any case the simultaneous V_p and SSA of MDCD are remarkably high and have not been observed in any other type of porous solids (e.g., up to 4.4 cm^3 g^{-1} is reported in porous silica,[16] MOFs,[24] and other MOF-derived carbons[23]) so far. The SEM and TEM images show the surface morphology and carbonization induced turbostratic graphitic regions of 3D networks in MDCM (**Figure 2** and Figure S5, Supporting Information). The high-resolution SEM images of MDCM before and after TEPA loading show further insights of the local pore structures. The hierarchical pores with large cavities and microcracks can facilitate easy amine loading into most of the pores. The 4.0TEPA@MDCM still shows some degree of free internal volume, which can aid rapid mass transport of CO_2 molecules. ActGO shows that the pores are well below 10 nm with SSA and total V_p of ≈2500 m^2 g^{-1} and ≈1.9 cm^3 g^{-1}, respectively. Thus as illustrated in Figure 1C, MDCM is clearly advantageous over ActGO in loading a high level of amines. According to the TEPA density (≈1 g cm^{-3}), the pores can accommodate up to 5 and 2 g of amine for each gram of MDCM and ActGO, respectively. Up to 6 g g^{-1} of TEPA loading in MDCM is easily obtained, whereas

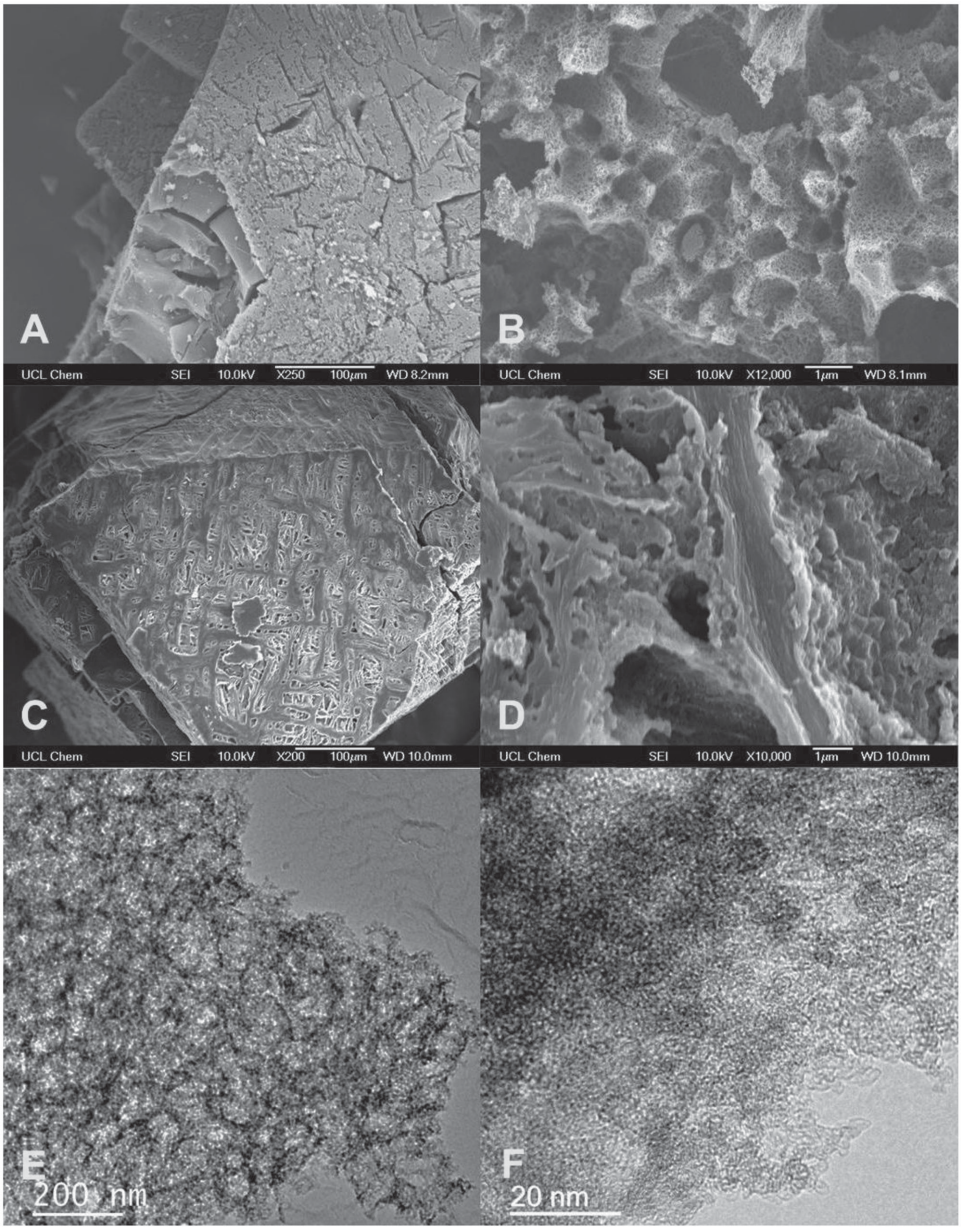

Figure 2. Surface morphology and pore structure of MDCM before and after TEPA impregnation. SEM images of a,b) MDCM and c,d) 4.0TEPA@MDCM, respectively. e,f) TEM images of MDCM. a,c,e) Low and b,d,f) high magnifications, respectively.

3 g g^{-1} of TEPA loaded ActGO sample becomes rather sticky (Figure 1C and Figure S6, Supporting Information). This is also evident from the direct comparison of the nitrogen isotherms (Figure S7, Supporting Information) and the derived porosity (Table S1, Supporting Information). Note that the reduction in pore volume with amine loading is larger than theoretical estimation based on amine liquid density, which may be directly attributed to the pore blocking effect.

The samples are further characterized by thermogravimetry (TG), Raman, Fourier transform infrared (FTIR), and X-ray photoemission spectroscopy (XPS). The major mass loss in TG plots (**Figure 3**A and Figure S8, Supporting Information) at >200 °C confirms the amine decomposition, which clearly suggests a relatively high thermal stability (≈100 °C) of the impregnated amine compared with the bulk counterpart. Porosity enhanced thermal stability is also greater in MDCM than in ActGO. It is remarkable that the Raman spectra still show representative Raman modes of host carbon even in the 6 g g^{-1} TEPA loaded sample (Figure S9, Supporting Information). The excess amine coating on surface is evidenced at smeared out D and G modes with a highly increased background. FTIR shows very weak IR absorption modes of TEPA in most of the MDCM compared with ActGO (Figure 3B and Figure S10, Supporting Information). This is directly attributed to the well-confined phase of TEPA that is highly dispersed within the pores of MDCM compared to excess surface coating of bulk TEPA in

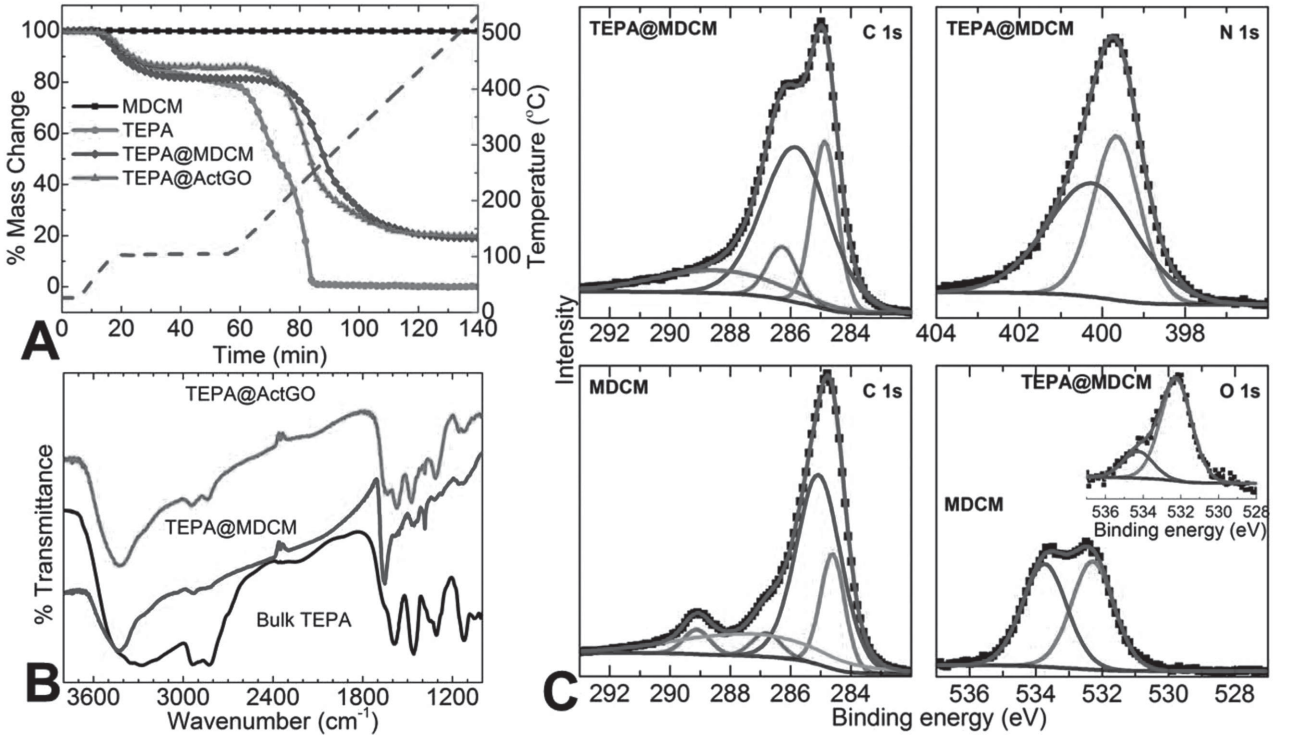

Figure 3. Thermal stability and spectroscopic characteristics of TEPA loaded MDCM and ActGO. A) TG plots and B) FTIR spectra of 4.0TEPA@MDCM and 4.4TEPA@ActGO; MDCM and bulk TEPA are also measured for a reference. C) XPS C 1s, N 1s, and O 1s spectra of MDCM and 4.0TEPA@MDCM. The square solid data are experimental and solid lines are deconvoluted peak fittings. Inset is O 1s spectrum for TEPA@MDCM.

ActGO. In addition, the redshift (decrease in frequency) and blueshift of N—H and C—H modes, respectively, from bulk to impregnated TEPA confirm the pore confinement and interactions with MDCM/ActGO supports. The amine interaction is also evident in the shifts of —OH and C=C/C=O stretching in MDCM/ActGO. In XPS (Figure 3C and Figure S11, Supporting Information), the deconvolution of C 1s spectrum of MDCM shows a combination of graphitic sp^2 and defective sp^3 carbons with considerable C—O and —COOH (or —OH—C=O) functionalities, which is also seen in O 1s two-peak behavior. After amine loading a clear change in C 1s and O 1s spectra is seen due to the amine C—N bonds and coordinated oxygen between C and amine. The peak fitting of N 1s suggests more or less equal two peaks at ≈399.6 and ≈400.2 eV, corresponding to free and surface bound amines, respectively.

Next the CO_2 uptake in all samples is screened with dry CO_2 of 100% with low pressure volumetric sorption isotherms measured between 60 and 75 °C on a Quantachrome gas uptake analyzer (Figure S12, Supporting Information). As shown in **Figure 4**A the uptake is mainly governed by amine loading. The amine loading between 4 and 5 g g^{-1} shows an optimum or the highest CO_2 uptake, again correlating well with the support (MDCM) pore volume. Either side of this loading shows a reduced uptake, in good agreement with the amine content in the free pore space and thickened surface coating of bulk amine outside the filled pores, respectively. Similar trend is also observed in amine@ActGO, about 2 g g^{-1} amine loading is the optimum. Importantly, the CO_2 uptake value of over 6 mmol g^{-1} at 1 bar in 4.0TEPA@MDCM is comparatively very high to any known amine@carbon and is comparable with or higher than other amine@silica systems known to date (see Table S2 in the Supporting Information).[9,15–22,27–31] Most of the literature on amine@solid sorbents shows a maximum possible CO_2 capacity well under 6 mmol g^{-1}. Here, a notably high CO_2 uptake of 5.6 mmol g^{-1} is observed at a low CO_2 pressure of 0.15 bar, whereas the highest CO_2 uptake reported in any type of amine@carbon is 4.8 mmol g^{-1}, obtained by breakthrough experiment in a 3.0PEI@carbon again due to a high pore volume of ≈3.6 cm^3 g^{-1} and a wide range of pores between 20 and 30 nm in the carbon support.[22] Most of the commercial silica/activated carbons show smaller pore sizes, between 2 and 10 nm and pore volumes, mostly between 1 and 2 cm^3 g^{-1} (Tables S1 and S2 in the Supporting Information). Thus, the unique pore characteristics in the MDCM are the key for achieving high amine confinement and contribute to this outstanding CO_2 uptake capacity. The maximum capacity of 6.1 mmol g^{-1} in 4.0TEPA@MDCM shows the amine efficiency of ≈0.29 mol CO_2 per mol N, comparable to or higher than other amine@silica samples.[17] The heat of adsorption of ≈50 kJ mol^{-1} at the CO_2 uptake of 4.4 mmol g^{-1} for the 3.6TEPA@MDCM (Figure S12, Supporting Information) is almost 50% lower than that of an aqueous amine sorbent of 30% monoethanolamine (≈100 kJ mol^{-1}).[7,14,17]

The cyclic lifetime on repeated adsorption–desorption runs is measured on TG with 100% CO_2 and N_2, and at simulated flue gas conditions. For example, **Figure 5**A represents characteristic flue gas CO_2 cyclic uptake curves between 5th and 16th cycles of a total of 20 during a 45 h operation (see Figure S13

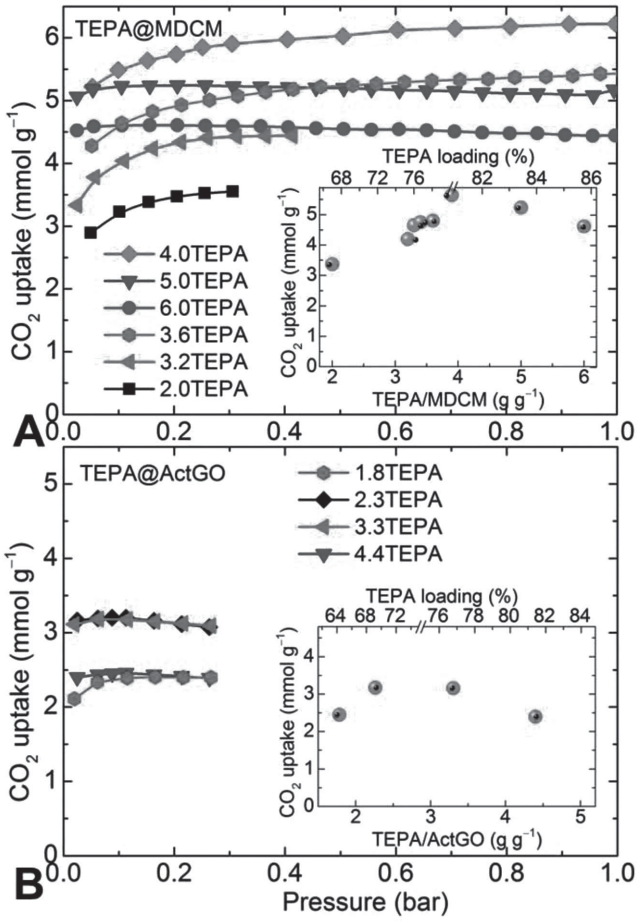

Figure 4. CO_2 uptake isotherms measured at 75 °C against TEPA loading. A) TEPA@MDCM, the upward and downward slopes of the isotherms either side of the TEPA loading of 4 g g^{-1} are in good agreement with the V_p value of MDCM, i.e., a Langmuir-type isotherm due to remaining microporosity and completely filled/blocked pores, respectively. B) TEPA@ActGO. Insets in (A) and (B) show variation of CO_2 uptake at 0.15 bar CO_2 as a function of TEPA loading. The effective CO_2 uptakes are achieved at more or less pore volume equivalent TEPA loading.

in the Supporting Information). The pre-assessed kinetics and uptake capacity tests at 60–90 °C (Figure S14 and S15, Supporting Information) show 75–80 °C is the optimum for rapid uptake, reaching over 90% within 2 min compared to a few hours for bulk TEPA. Figure S13 (Supporting Information) shows comparatively full cyclic test runs up to 20 cycles at similar experimental conditions for both MDCM and ActGO-based samples. A clear advantage is seen for the MDCM system over ActGO in terms of cyclic life, total uptake capacity, and sorption kinetics (Figure S14, Supporting Information). As shown in Figure 5B the capacity loss is just about 6% between the 2nd and the 20th cycle for 5.0TEPA@MDCM, whereas under a similar situation, the loss accounts for 17% and 36% in 6.0TEPA@MDCM and 4.4TEPA@ActGO, respectively. Earlier in the literature a notable capacity loss up to 23% within first 5–10 cycles is reported for TEPA loadings as small as 1–1.5 g g^{-1} in silica and clay supports (Figure S16 and Table S2, Supporting Information). For instance, 1.5TEPA@sepiolite clay shows up to 14% capacity loss within the first ten cycles even with a low temperature, 90 °C desorption runs.[11]

Furthermore, the long cyclic stability, up to 82 test runs of the sorbent is demonstrated with 100% CO_2. Figure 5C shows the characteristic curves between 41st and 56th cycles of the total runs in a 70 h operation (Figure S17, Supporting Information). As a reference we also measured cyclic N_2 uptake, which is just about 2 wt% (Figure S17C, Supporting Information). A remarkable cyclic uptake stability is seen in Figure 5D, where it compares with four other TEPA@silica systems from the literature. It is clear that in the mesoporous silica, such as MCM-41, SBA-15, and monoliths, a rapid uptake capacity loss up to 11% is observed within first seven or fewer cycles for a given TEPA loading of 1–2 g g^{-1}.[20,29,30] The silica capsules show slightly high initial cyclic stability, which could be due to its relatively high surface area for amine interaction.[18] However, a rapid capacity loss is seen at longer runs, ultimately the system shows about 40% of capacity loss at 50th cycle with 5 g g^{-1} TEPA loading. In any case, the capacity loss is primarily attributed to the loss of amine on repetitive desorption at ≥75–100 °C for the system. The amine loss is also observed in much more stable poly/branched amines in silica.[17,19,31] For instance, a cyclic capacity loss of ≈29% is reported in a mesoporous silica foam loaded with PEI (of 80 wt%) after 100 cycles of temperature swing.[17] This is directly attributed to the loss of amine, where the system mass loss accounts about 30%. It is expected because of the thick layer of excess amine coating on the outer pore surface that is prone to leach out of the sample easily.

For a total pore volumes of ≤1 cm^3 g^{-1} in silica (MCM-41, SBA-15, and silica foam/capsules; see Table S2, Supporting Information) and according to the density of TEPA or PEI (≈1 g cm^{-3}) it is possible to load about 1 g g^{-1} amine within the pores. Therefore, any excess amount of amine loading of >1 g g^{-1} resides on the particle external surface. For example, almost 3–5 g g^{-1} of amine out of the total loading of 4–6 g g^{-1}, ≈70–86%, is covered on the silica particle surface. In case of the MDCM most of the TEPA is well impregnated within the pores. Interestingly, a considerable amine loss is also observed in mesoporous silica even at pore volume equivalent amine loadings, i.e., 1 g g^{-1}, ≈50% amine. Therefore, compared with the 1D pores of silica, the highly hierarchical, 3D pores in MDCM act as near space-filling networks (see TEM images in Figure 2 and Figure S5 in the Supporting Information) for strong confinement of impregnated amine thus leading to high amine stability. Indeed, this is well in accord with the initial and final sample masses at the beginning and the end of the cyclic desorption runs. As a further note, the sample mass loss in 5.0TEPA@MDCM and 4.0TEPA@MDCM after 20 and 90 cycles, respectively, is just about 7% and 12%, compared to 16% in 4.4TEPA@ActGO. The hierarchical pore enhanced amine stability is further supported by a comparative study on PEI loaded hybrid graphene–silica sheets with hierarchical pores and pure silica sheets with a uniform 1D pores.[31] The PEI on graphene–silica becomes very stable for the first 20 cycles of temperature swing, whereas at the same experimental conditions the PEI–silica shows ≈28% capacity loss. Another important advantage in using the graphenic carbon support is their superior heat dissipation capability over relatively poor thermal conduction of mesoporous silica.[31] As CO_2 interaction with amines is

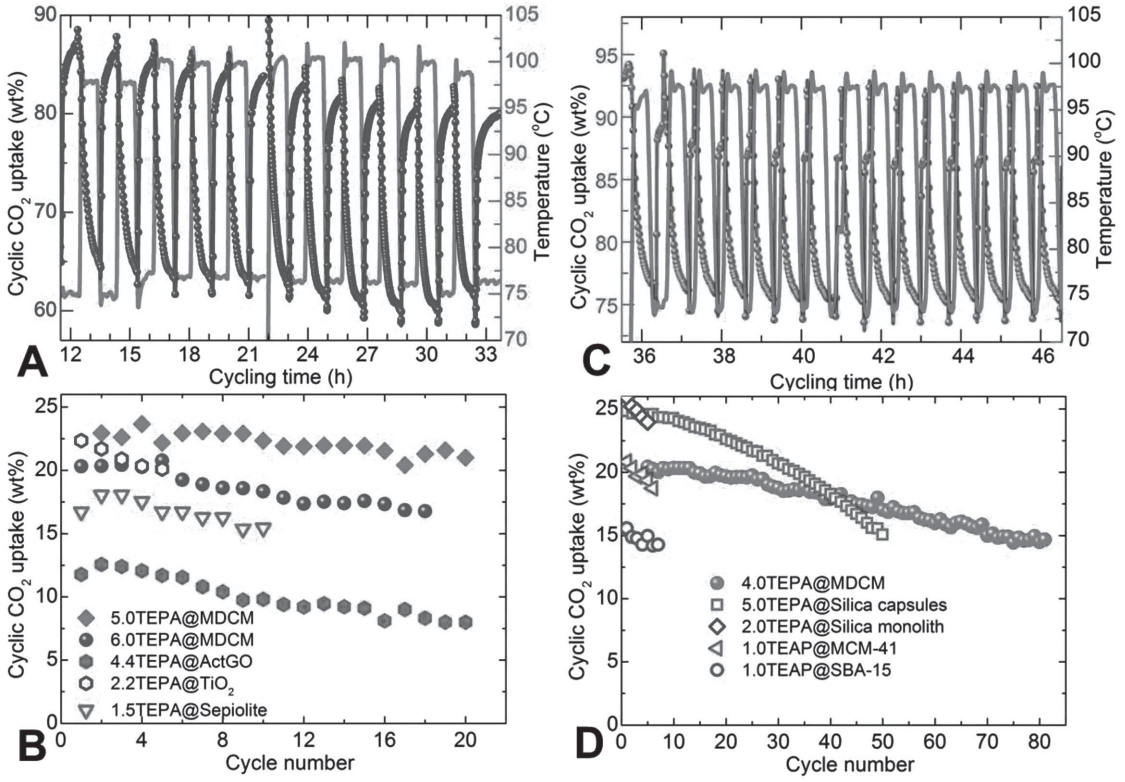

Figure 5. Cyclic CO_2 uptake characteristics at 75 °C with 100 °C desorption. A) Simulated flue gas uptake (15% CO_2 in 85% N_2: flowing through a water bubbler at 50 mL min^{-1}) cyclic curves between 5th and 16th cycles of 5.0TEPA@MDCM with equal sorption and desorption time of 50 min. B) Cyclic uptake capacity and stability under simulated flue gas, up to 20 runs, for 5.0TEPA@MDCM (solid diamonds), 6.0TEPA@MDCM (solid spheres), 4.4TEPA@ActGO (solid hexagons), 2.2TEPA@TiO_2 nanotubes (open hexagons, at 60 °C)[28] and 1.5TEPA@sepiolite (open triangles, at 60 °C).[11] C) Cyclic uptake at 100% CO_2 (humidified) between 41st and 56th cycles for 4.0TEPA@MDCM with 10 min sorption and 20 min desorption. D) Cyclic uptake capacity and stability at 100% CO_2 up to 82 runs for 4.0TEPA@MDCM (solid spheres), 5.0TEPA@silica capsules (open squares, 10 min each for sorption–desorption at 75–100 °C),[18] 2.0TEPA@silica monoliths (open diamonds, 100 min each sorption–desorption at 75 °C),[20] 1.0TEPA@MCM-41 (open triangles, 30 min desorption at 100 °C),[29] and 1.0TEPA@SBA-15 (open circles, 30 min desorption at 100 °C).[30]

exothermic, the carbon support can quickly dissipate the heat and prevent the chance of volatilization of amine.[5]

The samples subjected to CO_2 cycling are further characterized with FTIR and XPS. As shown in Figure S18 (Supporting Information), the FTIR shows prominent additional absorption modes between 1680 and 1630 cm^{-1}, suggesting partial oxidation of the samples.[32,33] This is also evidenced in the N 1s and O 1s peak shifts of XPS spectra (Figure S19, Supporting Information). Interestingly, this oxidation is more pronounced in a TEPA@ActGO than the TEPA@MDCM. Overall, it is very convincing that the excess amine coating on the surface outside the support pores is a major culprit and responsible for the rapid capacity loss. It is also understood that such amines are more susceptible to both oxidation and amine loss on repetitive adsorption–desorption cycles. Thus as shown above it is important to have not only a sufficiently high surface area, but also high pore volume with a wide range of 3D hierarchical pores spanning over the micro- to mesopore range in order to achieve near-space filling, strong confinement, and well dispersion of the impregnated amine. Further improvements may also be achieved by fine control of the pore size of the support. As an example we show that (Figure S20, Supporting Information) the pore size and its distribution can be limited by size-control of MOF crystals.[23,25] Other strategies, such as gentle compression and pore decoration with graphene foam,[31] can also enhance the mesopore density in the large cavities and free-void spaces of MDCM (see SEM images, Figure 2 and Figure S5, Supporting Information). The SEM images also show that there is still some degree of bulk deposition of the amine in the large pore space of MDCM. Thus, further control over confinement and distribution of impregnated amine within the mesopores can enhance the long-term thermal stability and capture capacity of the solid-amine@carbon sorbent. In addition, the surface area and micropores can facilitate rapid mass transport and diffusion channels for CO_2 therefore very fast kinetics of adsorption and desorption can be achieved.[34]

In summary, we have discovered a carbon-monolith-based solid-amine system for efficient CO_2 capture. Important insights on the cyclic CO_2 uptake and amine stability of solid-amine sorbents are presented. The MOF-derived carbon monoliths exhibit an ultrahigh hierarchical pore volume of 5.35 $cm^3\ g^{-1}$, with a simultaneously high surface area up to 2700 $m^2\ g^{-1}$, and are able to accommodate a record high level of amine, up to 5 g g^{-1} within its hierarchically networked micro/mesopores over a wide range. On the other hand, for the same level of amine loading, over 60% of the amine content resides on the external

surface of already filled pores in the carbon/silica supports with a pore volume of ≤2.0 cm^3 g^{-1}. Thus, the highly dispersed and stabilized TEPA within the hierarchical 3D pore structure of MDCM shows much enhanced flue gas CO_2 scrubbing properties with remarkably stable long cyclic life. The results also suggest that the high capacity solid-amine-based sorbents for CO_2 scrubbing can be obtained by the designing the support with a high pore volume. The long-term and high-temperature stability can be further enhanced with the incorporation of the more stable long chain and high molecular weight polyamines, for example, pentaethylenehexamine. Furthermore, the control over CO_2 uptake and release is attainable with fine-tuning of pore structures of the host carbon. The ultimate issue may be not to divest in fossil fuels, but to invest in effective and efficient carbon capture for fossil fuels.

Supporting Information

Supporting Information is available from the Wiley Online Library or from the author.

Acknowledgements

This work was supported by the EPSRC (Grant Nos. EP/J020745/1 and EP/G063176/1). The authors would like to thank Tingting Zhao and Steve Firth for assistance with SEM and TEM imaging.
Note: Several typographical errors were corrected on September 2, 2015, after initial publication online. Also, the volume and page numbers were added in reference 25.

Received: April 29, 2015
Revised: June 8, 2015
Published online: July 14, 2015

[1] *International Energy Agency (IEA), Report on CO2 Emissions From Fuel Combustion Highlights*, **2014**; available from: https://www.iea.org/publications/freepublications/publication/CO2EmissionsFromFuelCombustionHighlights2014.pdf, accessed: June 2014.
[2] B. Booth, N. Bellouin, *Nature* **2015**, *519*, 167.
[3] M. E. Boot-Handford, J. C. Abanades, E. J. Anthony, M. J. Blunt, S. Brandani, N. M. Dowell, J. R. Fernández, M.-C. Ferrari, R. Gross, J. P. Hallett, R. S. Haszeldine, P. Heptonstall, A. Lyngfelt, Z. Makuch, E. Mangano, R. T. J. Porter, M. Pourkashanian, G. T. Rochelle, N. Shah, J. G. Yao, P. S. Fennell, *Energy Environ. Sci.* **2014**, *7*, 130.
[4] G. T. Rochelle, *Science* **2009**, *325*, 1652.
[5] A. I. Cooper, *Nature* **2015**, *519*, 294.
[6] G. Sneddon, A. Greenaway, H. H. P. Yiu, *Adv. Energy Mater.* **2014**, *4*, 1301873.
[7] a) K. Sumida, D. L. Rogow, J. A. Mason, T. M. McDonald, E. D. Bloch, Z. R. Herm, T.-H. Bae, J. R. Long, *Chem. Rev.* **2012**, *112*, 724; b) S. Choi, J. H. Drese, C. W. Jones, *ChemSusChem* **2009**, *2*, 796; c) A. Samanta, A. Zhao, G. K. H. Shimizu, P. Sarkar, R. Gupta, *Ind. Eng. Chem. Res.* **2012**, *51*, 1438; d) M. L. Gray, J. S. Hoffman, D. C. Hreha, D. J. Fauth, S. W. Hedges, K. J. Champagne, H. W. Pennline, *Energy Fuels* **2009**, *23*, 4840.
[8] S. Gadipelli, Z. X. Guo, *Prog. Mater. Sci.* **2015**, *69*, 1.
[9] J. Wang, L. Huang, R. Yang, Z. Zhang, J. Wu, Y. Gao, Q. Wang, D. O'Hare, Z. Zhong, *Energy Environ. Sci.* **2014**, *7*, 3478.
[10] T. M. McDonald, J. A. Mason, X. Kong, E. D. Bloch, D. Gygi, A. Dani, V. Crocellà, F. Giordanino, S. O. Odoh, W. S. Drisdell, B. Vlaisavljevich, A. L. Dzubak, R. Poloni, S. K. Schnell, N. Planas, K. Lee, T. Pasca, L. F. Wan, D. Prendergast, J. B. Neaton, B. Smit, J. B. Kortright, L. Gagliardi, S. Bordiga, J. A. Reimer, J. R. Long, *Nature* **2015**, *519*, 303.
[11] M. Irani, M. Fan, H. Ismail, A. Tuwati, B. Dutcher, A. G. Russell, *Nano Energy* **2015**, *11*, 235.
[12] W. Lu, M. Bosch, D. Yuan, H.-C. Zhou, *ChemSusChem* **2015**, *8*, 433.
[13] B. Dutcher, M. Fan, A. G. Russell, *ACS Appl. Mater. Interfaces* **2015**, *7*, 2137.
[14] G. Qi, L. Fu, E. P. Giannelis, *Nat. Commun.* **2014**, *5*, 5796.
[15] C. Chen, J. Kim, W.-S. Ahn, *Korean J. Chem. Eng.* **2014**, *31*, 1919.
[16] H. Zhang, A. Goeppert, M. Czaun, G. K. S. Prakash, G. A. Olah, *RSC Adv.* **2014**, *4*, 19403.
[17] G. Qi, L. Fu, B. H. Choi, E. P. Giannelis, *Energy Environ. Sci.* **2012**, *5*, 7368.
[18] G. Qi, Y. Wang, L. Estevez, X. Duan, N. Anako, A.-H. A. Park, W. Li, C. W. Jones, E. P. Giannelis, *Energy Environ. Sci.* **2011**, *4*, 444.
[19] A. Goeppert, S. Meth, G. K. S. Prakash, G. A. Olah, *Energy Environ. Sci.* **2010**, *3*, 1949.
[20] C. Chen, S.-T. Yang, W.-S. Ahn, R. Ryoo, *Chem. Commun.* **2009**, 3627.
[21] W. Zhang, H. Liu, C. Sun, T. C. Drage, C. E. Snape, *Chem. Eng. J.* **2014**, *251*, 293.
[22] J. Wang, H. Chen, H. Zhou, X. Liu, W. Qiao, D. Long, L. Ling, *J. Environ. Sci.* **2013**, *25*, 124.
[23] G. Srinivas, V. Krungleviciute, Z.-X. Guo, T. Yildirim, *Energy Environ. Sci.* **2014**, *7*, 335.
[24] H. Furukawa, K. E. Cordova, M. O'Keeffe, O. M. Yaghi, *Science* **2013**, *341*, 974.
[25] S. Gadipelli, Z. X. Guo, *ChemSusChem* **2015**, *8*, 2123.
[26] S. J. Yang, T. Kim, K. Lee, Y. S. Kim, J. Yoon, C. R. Park, *Carbon* **2015**, *71*, 294.
[27] D. Wang, X. Ma, C. Sentorun-Shalaby, C. Song, *Ind. Eng. Chem. Res.* **2012**, *51*, 3048.
[28] F. Song, Y. Zhao, Y. Cao, J. Ding, Y. Bu, Q. Zhong, *Appl. Surf. Sci.* **2013**, *268*, 124.
[29] M. B. Yue, L. B. Sun, Y. Cao, Y. Wang, Z. J. Wang, J. H. Zhu, *Chem. Eur. J.* **2008**, *14*, 3442.
[30] M. B. Yue, Y. Chun, Y. Cao, X. Dong, J. H. Zhu, *Adv. Funct. Mater.* **2006**, *16*, 1717.
[31] S. Yang, L. Zhan, X. Xu, Y. Wang, L. Ling, X. Feng, *Adv. Mater.* **2013**, *25*, 2130.
[32] A. Sayari, A. Heydari-Gorji, Y. Yang, *J. Am. Chem. Soc.* **2012**, *134*, 13834.
[33] C. S. Srikanth, S. S. C. Chuang, *ChemSusChem* **2012**, *5*, 1435.
[34] J. J. Vericella, S. E. Baker, J. K. Stolaroff, E. B. Duoss, J. O. Hardin IV, J. Lewicki, E. Glogowski, W. C. Floyd, C. A. Valdez, W. L. Smith, J. H. Satcher Jr., W. L. Bourcier, C. M. Spadaccini, J. A. Lewis, R. D. Aines, *Nat. Commun.* **2015**, *6*, 6124.